ANNALS OF GEOPHYSICS, 65, 4, VO429, 2022; doi:10.4401/ag-8807
OPEN ACCESS

Monitoring magma migration at Mt. Etna using the Seismic Amplitude Ratio Analysis method

Ghazaleh Rasaneh[1], Alireza Hajian[*,1], Maryam Hodhodi[1], Roohollah Kimiaefar[1] and Salvatore Gambino[2]

(1) Department of Physics, Najafabad Branch, Islamic Azad University, Najafabad, Iran
(2) Istituto Nazionale di Geofisica e Vulcanologia, Osservatorio Etneo, Catania, Italy

Article history: received February 16, 2022; accepted April 24, 2022

Abstract:

The Seismic Amplitude Ratio Analysis method (SARA) was applied to data recorded during six days before the May 13, 2008 eruption of Mt. Etna to test its potential as a forecasting attribute. By using this method, the magma migration path, as well as the seismic migration, can be determined with the amplitude of continuous data recorded at least at one pair of stations from a seismic network near the eruption site. Due to the sudden changes in the seismic amplitude ratio calculated for each pair of stations, the seismic migration trend, as well as the magma path at depths, were clearly detected before the main eruption. The start and end times of the seismic swarms were also determined. The standard practice to achieve similar results is to use volcanic tremors, which must be pre-selected thus reducing efficiency and increasing the time needed. By using the whole seismic signal, the method provides a simpler semi-automated alternative, especially for places where it is not possible to record tremors continuously. This simple method is useful to reduce uncertainties relative to hazardous magma propagation during volcanic unrest, as it helps to improve the accuracy of locating seismic swarms and it allows determining the direction of magma movement at depth before the eruption. We also analyzed the amplitude ratio trend using Mann-Kendall and Sen's estimator test. The results of these tests confirmed a positive and increasing trend from the day before the eruption in most pairs of stations.

Keywords: Magma migration; Seismic Amplitude Ratio Analysis; Etna volcano; Eruption; Seismic swarms

1. Introduction

Creating a reliable scientific platform for regular and inexpensive volcanic monitoring is an important task on a global level. Estimating the dynamic of magma migration and seismic swarms before eruptions are one of the most effective seismic methods for volcanic monitoring.

One way to track magma movement before an eruption is using seismic signals. Seismic swarms are a common occurrence at volcanoes around the world and are often accompanied by periods of increasing volcanic activity. The severity and extent of seismic swarms before eruptions have led to their use in forecasting eruptions.

In the Seismic Amplitude Ratio Analysis method (SARA), the amplitudes recorded in different stations are used to determine the location of accumulated seismic energy and its migration path. In the absence of an earthquake, stations can continuously detect and locate seismic energy, making SARA a practical method for volcano monitoring [Tan et al., 2019]. Earthquake localization using the SARA method was originally introduced as an alternative to overcome the limitations of traditional earthquake location methods, without the need for phase picking, especially during seismic swarms [Battaglia et al., 2005]. Later, in addition to locating earthquakes, this method was applied to determine the movement of magma before the eruption i.e., for the volcanoes: Piton de la Fournaise [Taisne et al., 2011], Tolbachik [Caudron et al., 2015], Bardarbunga and Hoiuhraun [Caudron et al., 2018], Virunga [Subria et al., 2019] and good results were achieved that correctly indicated the path of magma migration, before the related main eruptions. Tan et al. [2020] introduced a modified method called Red-flag SARA, which also calculated temporal changes in slope ratios, and implemented this method on Piton and Gede volcanoes. By performing this method, they examined the migration of magma in three stages: 1) Magma migration leading to intrusion 2) Magma migration leading to the eruption and 3) Seismic migration without magma migration. It should be noted that as the Red-flag SARA method is based on a statistical approach, the records from many more stations are required.

As the Etna Volcano is the largest active volcano in Europe and one of the best monitored volcanoes in the world, many articles have been presented on various methods to monitor and track the magma before an eruption, as well as assessing the related risk. Aloisi et al. [2009] used continuous GPS data from May 2008 to December 2010 and analyzed them in order to assess the volcanic hazard and model the active sources of the Etna volcano. Crisci et al. [2010] used a computational model to simulate the flow of lava before an eruption occurred and predict the eruption time. Barreca et al. [2013] also performed three-dimensional modeling of Mount Etna to evaluate the volume and trend of the eruption rate, by calculating the amount of magma emitted over time. Viccaro et al. [2016] used a combination of geodetic, seismic and petrological data, to estimate the location and time of magma migration before the eruption. Aloisi et al. [2017] investigated how increased stress in the region due to seismic swarms could cause more magma activity and eventually an eruption in Mount Etna. De Plaen et al. [2019] investigated the possibility of tracking the temporary changes in the velocity of seismic waves before the main eruptions of Etna using autocorrelation of ambient noise and developed a tool for volcano monitoring. Also, Laiolo et al. [2019] by combining satellite, infrasonic and seismic tremor data, tracked the shallow magma movement in Etna.

In this research, the SARA method was applied to the 2008 Etna main eruption. The main reason for selecting this eruption was that it is one of the most significant and intense eruptions of Etna with extensive studies and there was a good possibility to compare the previous results with the results of this research in the field of volcano activity monitoring.

2. Chronology of the eruption

Etna is located on the east coast of Sicily, Italy, and is the highest active volcano in Europe. This is a hybrid volcano that formed at the intersection of two fault systems [Lo Giudice et al., 1982]. The volcanic activity of Mt. Etna includes continuous activity at the summit, with episodic paroxysmal events and flank eruptions that are preceded by intrusive seismic swarms and ground deformation [Allard et al., 2006; Gambino et al., 2018; Hajian et al., 2019]. The permanent seismic network of Mount Etna consists of 33 broadband stations and 12 short-term stations run by the Istituto Nazionale di Geofisica e Vulcanologia Osservatorio Etneo (INGV-OE). In this study, the seismic data of three stations (EBEL, EPDN and EPLC) were used to analyze the ratio of amplitude (Figure 1). Each station is equipped with a three-component Trillium seismometer and has a sampling rate of 100 Hz [Cannata et al., 2013].

Between 2007 and early 2008, a process of activity was recorded by INGV-OE at Mount Etna, which climaxed on 13 May 2008. The eruption was accompanied by relatively intense seismic activity so that in the first 6 hours, about 230 seismic events occurred [Aloisi et al., 2009; Alparone et a., 2012; Bonaccorso et al., 2011a]. On 13 May, a new eruptive fissure opened between 3,050 and 2,650m elevation on Etna's upper eastern flank (as shown in Figure 2), feeding magma streams into the Valle del Bove. This eruption occurred after a recharge phase began in 2006 and was accompanied by numerous lava fountain episodes from the Southeast Crater (SEC) [Bonaccorso et al., 2011b; Wunderman et al., 2008].

Three days before the main eruption on 10 May 2008, one of the most intense activities of the volcano occurred due to the opening of a new vent at the eastern base of the SEC. A few hours before the start of the main eruption on 13 May, a shallow seismic swarm began at 8:39 in the morning and continued until 15:25. About 240 earth-

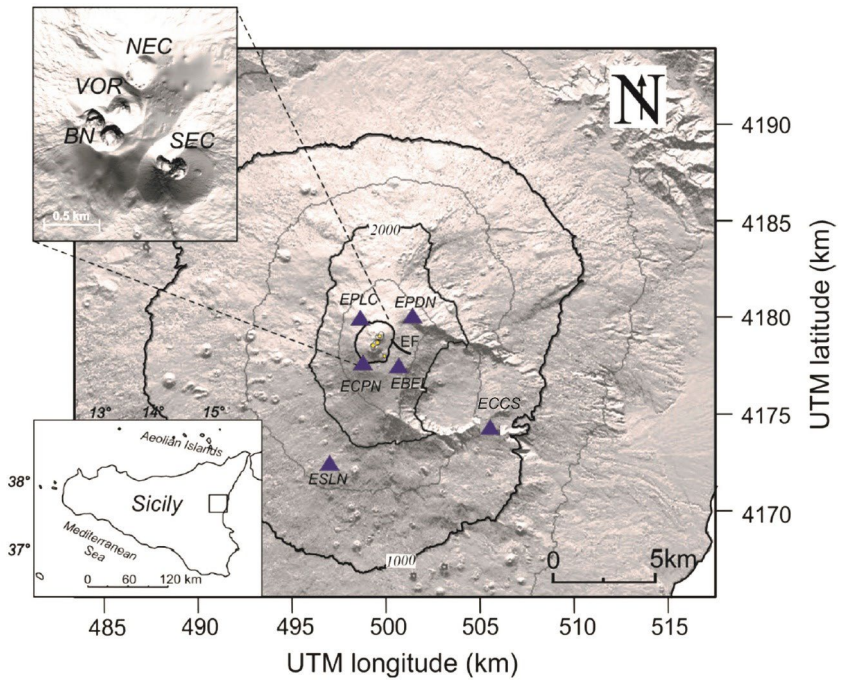

Figure 1. The digital elevation map of Mt. Etna with locations of the seismic stations; note that five of these stations were used in this study (EBEL, ECCS, EPDN, EPLC and ECPN). The distribution of the four summit craters by DEM is shown in the upper left corner of the image (VOR: Voragine, BN: Bocca Nuova, SEC: Southeast Crater, NEC: North-East Crater). The distance of EBEL from each of the summit craters (VOR, BN, SEC, and NEC) is 1.7, 1.8, 1.2, and 2 km, respectively [Redrawn after Spina et al., 2014].

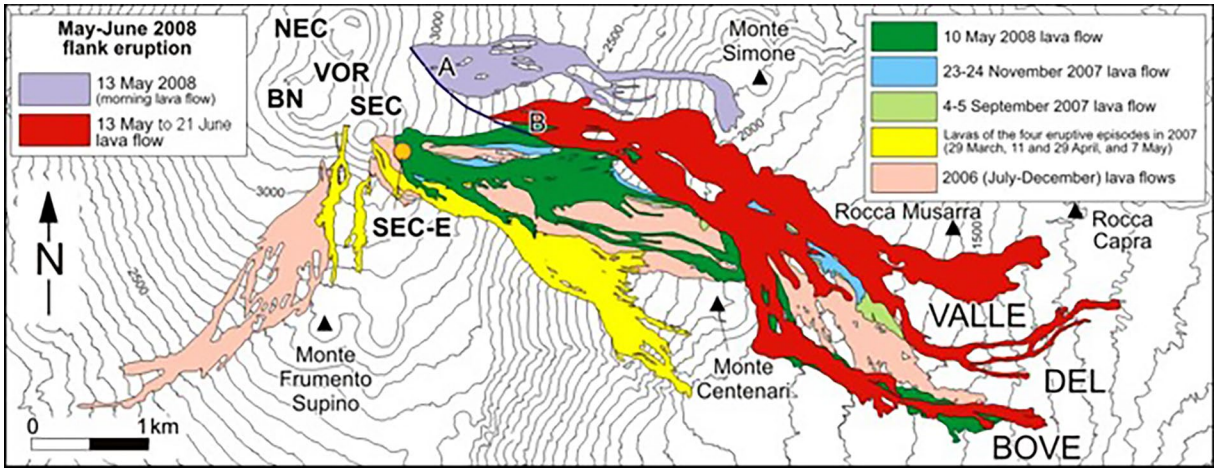

Figure 2. Map of the lava flows from 2006 to 2008, including the 2008 eruption. Summit craters are Northeast Crater (NEC), Bocca Nuova (BN), South East Crater (SEC), and Voragine (VOR), whose recently active vent on the E flank is labeled SEC-E. The upper E flank fissure system is prominent by two sections: (A) Active on the morning of 13 May. And (B) the activity of this part started from the afternoon of May 13 and continued until June. Courtesy of INGV-OE [Wunderman, 2008].

quakes were recorded during this period, most of which occurred in the first two hours of the eruption (as shown in Figure 3). These events were located in the north-eastern summit area at a depth between 1500 m b.s.l. and 1500 m a.s.l. The Spatio-temporal distribution of earthquakes showed a northward migration that was interpreted as a stopped shallow intrusion towards this sector of the volcano, confirmed by the propagation of non-eruptive fractures from the summit towards NNW [Wunderman, 2008].

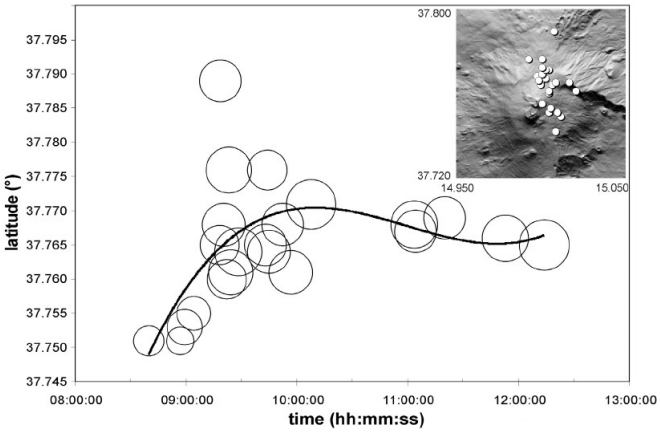

Figure 3. Location of seismic swarms that occurred before, during, and after the 13 May 2008 eruption of Etna volcano as a function of latitude versus time. The size of the circles is commensurate to the duration magnitude (M Dmin = 1.0, M Dmax = 3.3). Inset shows the map of the summit area with the position of the epicenters [from Bonaccorso et al., 2011].

The epicenter's time pattern evidenced an almost stationary distribution in the upper flanks of the Valle del Bove until 9:30 GMT. Thereafter, a clear migration of the seismic events occurred toward the top of the North-East Rift, suggesting a northward propagation of a magmatic intrusion. Earthquakes were accompanied by a gradual and intense increase in the intensity of volcanic tremors. The main release of seismic energy occurred up to 10:00 GMT when the tremor amplitude drastically decreased but returned to normal background levels only on 14 May [Bonaccorso et al., 2008].

3. Method

Seismic Amplitude Ratio Analysis (SARA) has been successfully used to track the subsurface migration of magma before the eruption of some volcanoes such as Piton de la Fournaise, Tolbachik, Bardarbunga, and Hoiuhraun. This method is based on calculating the ratio of recorded seismic amplitudes from each pair of stations and analyzing the results. The SARA method can show the migration of magma in a shallow part of the volcanic structure and is also used to locate volcanic earthquakes without needing to perform phase picking. Since these calculations use independent stations and the damping is likely to be eliminated in short periods of seismic swarms [Tan et al., 2019], any change in amplitude can be attributed to the displacement of the seismic source, which implies stress migration and ultimately magma migration. Considering amplitudes of the two different stations, the seismic amplitude ratio is calculated by [Caudron et al., 2015]:

$$\frac{A_1}{A_2} = \frac{A_2 cor}{A_1 cor} exp\left(-B(r_1 - r_2)\right)\left(\frac{r_2}{r_1}\right)^n \quad (1)$$

Where:

$B = \frac{\pi f}{Q\beta}$ and A_1 and A_2 are the seismic amplitudes at stations 1 and 2, respectively; $A_1 cor$ and $A_2 cor$ are the corrected amplitude at stations 1 and 2, respectively; r_1 and r_2 are the distances between the seismic source and stations 1 and 2, $n = 1$ for body waves and $n = 0.5$ for surface waves, β is the seismic wave velocity, Q is the Quality Factor for attenuation and f is the central frequency. We then seek a spatial location such that the theoretical ratios best fit the observed ones for the set of station pairs [Taisne et al., 2011].

In this study, shear wave velocity was used because the amplitude of S-waves is larger than that of body waves and also the S-wave radiation pattern was assumed to be isotropic at frequencies higher than 1 Hz [Battaglia and Aki, 2003; Takemura et al., 2009].

Natural logarithm (*ln*) of the amplitude ratio is used to better present and discuss the results:

$$Ln\frac{A_1}{A_2} = Ln\frac{A_2 cor}{A_1 cor}\left(-B(r_1 - r_2)\right) + nLn\left(\frac{r_2}{r_1}\right) \quad (2)$$

The appropriate values of Q and β were selected according to the seismicity and studies conducted in the region, as well as the frequency spectrum studied. Different values of site amplification factor for separate stations are used to calculate corrected amplitudes and find the best fit between observed corrected amplitudes and theoretical amplitudes.

To investigate the effect of the quality factor value on the trend of changes, the amplitude ratio of a pair of stations (EBEL/ECPN) on the day of the eruption (13 May 2008) was plotted with four different quality factors values (Figure 4). Selected quality factor values include maximum, minimum, and most frequently repeated values of this factor in articles related to the study area. [Del Pezzo et al., 2014; Patanè et al., 2008; Giampiccolo et al., 2007].

Figure 4 reveals that different values of the quality factor have no effect on the trend of changes in the amplitude ratio and only move the curves on the Ln scale. Finally, by selecting the appropriate values ($Q = 110, n = 1, \beta = 1000$ m/s) and determining the distance of the stations using the coordinates of seismic stations [Behncke.,2009], the amplitude ratio between each pair of stations was calculated theoretically using Eq. (1).

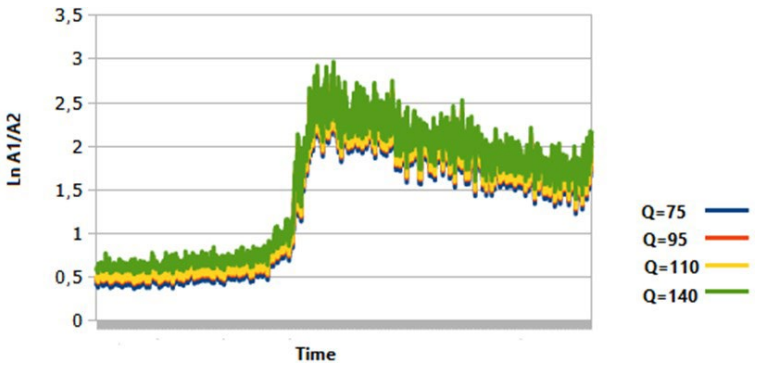

Figure 4. Theoretical ratios(A_1/A_2) between a pair of stations (EBEL- ECPN) for different Q values in main eruption day (13 May 2008).

4. Data Processing and Analysis

This study used continuous seismic data recorded from three stations EBEL, EPDN, and EPLC, that are close to each other and also close to the active craters (Figure 1). These stations are part of the volcano seismic network at the Istituto Nazionale di Geofisica e Vulcanologia, Osservatorio Etneo - Sezione di Catania (INGV-OE). The network consists of three-component broadband digital seismometers with a sampling rate of 100 Hz and cut-off period of 40 s. Here, we only used and processed the vertical component.

The data were processed by MSNoise software [Lecocq et al., 2014], and then the steps were performed by the Taisne method [2011]. The steps of data processing in this software are shown in Figure 5. After preparing and processing the data, the seismic amplitude ratio of each pair of stations was calculated and plotted using the SARA plugin in MSNoise software (as shown in Figure 6). The first stage of data processing involved preparing the waveforms for each station separately for checked quality and gaps (Figure 7). Then, the vertical components of daily recordings are divided into 30 min segments. In the next step, segments are demeaned and detrended, then traces are normalized to three times the root-mean-square (RMS) and spectrally whitened between 0.01 and 10 Hz. In the following, the daily cross-correlations between a pair of stations are computed. The cross-correlation function (CCF) is filtered between 5 to 15 Hz since, as suggested by [Laher 1994] because a large amount of energy is released in this frequency range. In the last step the amplitude ratios of each station pair are computed using summation over a one-minute window (see Table1).

Pre-process steps	Value
Analysis duration	86400 (S)
Decimation factor	5
Envelope sampling rate	1 (Hz)
High pass filter	5 (Hz)
Low pass filter	15 (Hz)
Pre-process sampling rate	20 (Hz)
Pre-process taper length	5 (S)

Table 1. Data pre-processing steps.

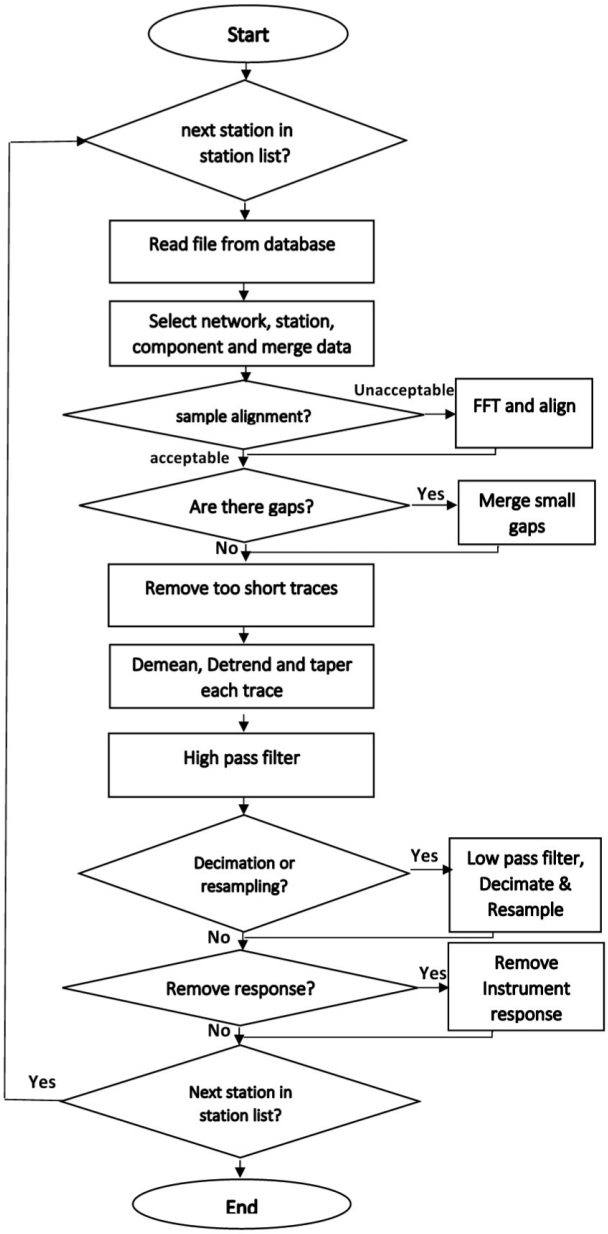

Figure 5. Flowchart of waveform pre-processing in SARA method [Lecocq et al., 2014].

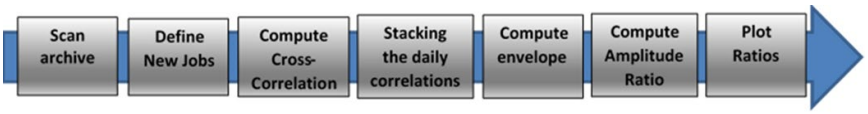

Figure 6. Workflow schematic view of the SARA plugin of MSNoise software.

To demonstrate the efficiency of the method, we focused on the Etna volcano eruption of 2008. Although the permanent seismic network around Etna volcano included 37 three-component trillium seismic stations [Alparone et al., 2012], only three of the closest stations to the NEC crater of Etna were selected. One of the important advantages of SARA's method is that it is not necessary to use all pairs of seismic stations and if eventually one or more stations in the network are damaged, this will not affect the results because the analysis can be implemented with a fewer number of stations.

We checked data for quality and possible gaps. As depicted in Figure 7, on 10 May 2008, there was a significant increase in the amplitude of the seismic signals at 14:00 UTC, indicating the beginning of a period of a paroxysmal eruption. Figure 8 shows that on the morning of 10 May, there is a significant change in the ratio of seismic

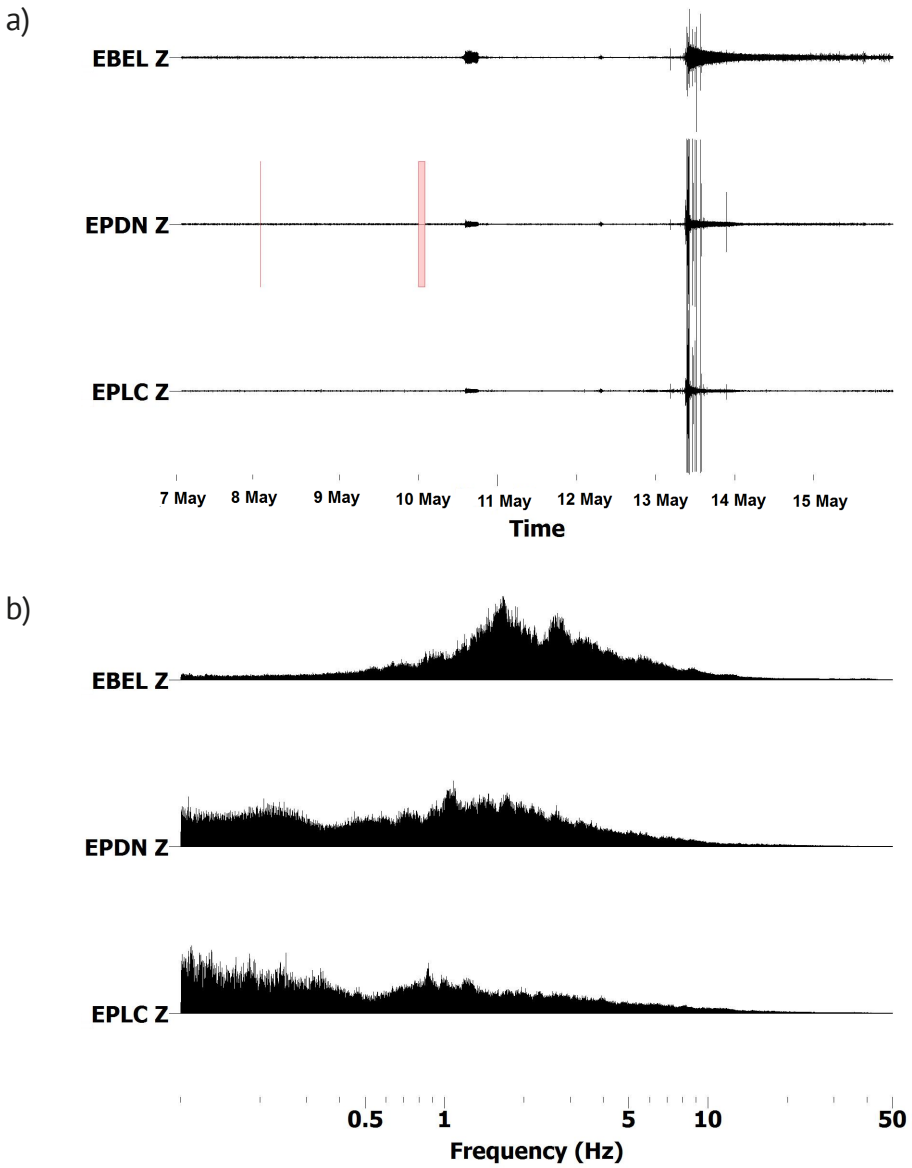

Figure 7. a) Waveforms of the three stations used in this study versus time. Waveforms are computed from the Z component of raw data with a sampling frequency of 100 Hz. b) Frequency spectrum related to part a.

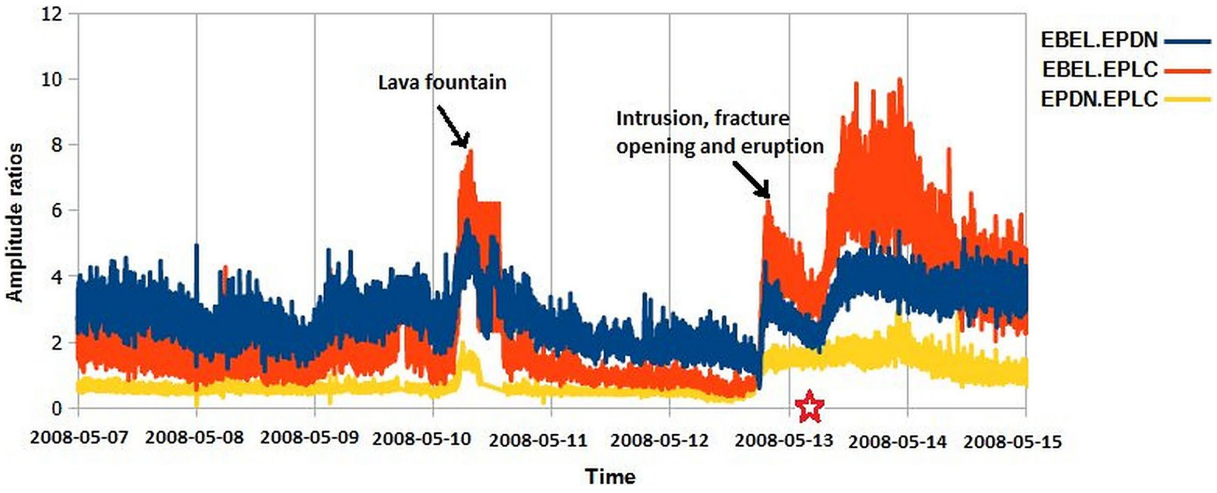

Figure 8. Seismic amplitude ratios: Seismic envelope calculated every second at EBEL, EPDN, and EPLC in the 5-15 Hz frequency band. Significant times are shown with black arrows and the time of the main eruption is shown with red stars. The amplitude ratio anomaly observed on 10 May is consistent with the lava fountain event.

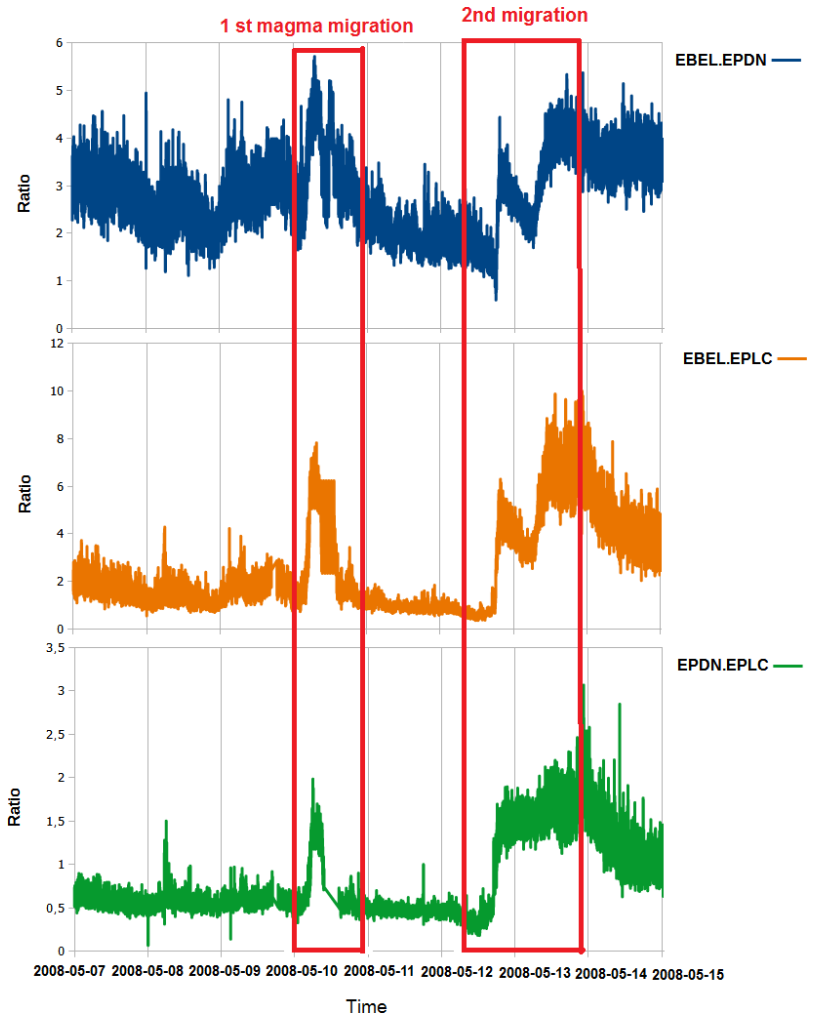

Figure 9. Seismic amplitude ratio charts of three pairs of stations (EBEL-EPDN, EBEL-EPLC, and EPDN-EPLC). The two periods of magma migration are shown by red lines.

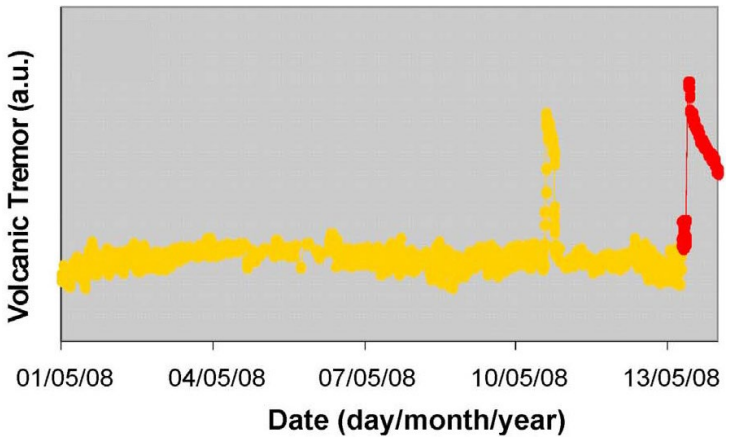

Figure 10. Volcanic tremor amplitude from 1 May 2008 to 13 May 2008. The red dots are related to the events recorded on the day of the eruption (May 13). The first sudden change in the amplitude of the tremors occurred on May 10, at the same time as the lava fountaining, and the second abnormality was observed on May 13, a few hours before the main eruption [from Bonaccorso et al., 2011].

amplitudes recorded at pairs of stations (EBEL/EPLC and EBEL/EPDN), which coincides with the lava fountain episode that began at 14:00 the same day. Studies show that the trend of amplitude ratios between stations does not depend on damping law but is a function of source location change [Caudron et al., 2015]. In this case, the ratio increase is caused by magma migration toward NEC where a paroxysm occurred and EBEL is the closest station to this crater. The most energetic phase, which shows the greatest changes in the ratio of seismic amplitudes recorded at the pairs of stations, occurred on the morning of 13 May, which coincides with the beginning of the intrusive seismic swarm, intrusion, fracture opening, and finally the main eruption (Figure 8). In the next step, the amplitude ratios of the three pairs of stations were calculated and the variations were plotted separately in three graphs (Figure 9). All three pairs of stations showed a sudden and temporary increase in the amplitude ratio before the lava foundation stage and main eruption. Although we used the whole seismic signal and did not limit ourselves to using tremors, the results are in good agreement with the results of similar articles that examined changes in the amplitude of tremors before the same eruption [Bonaccorso et al., 2011]. A comparison of Figure 10 with Figures 8 and 9 confirms this.

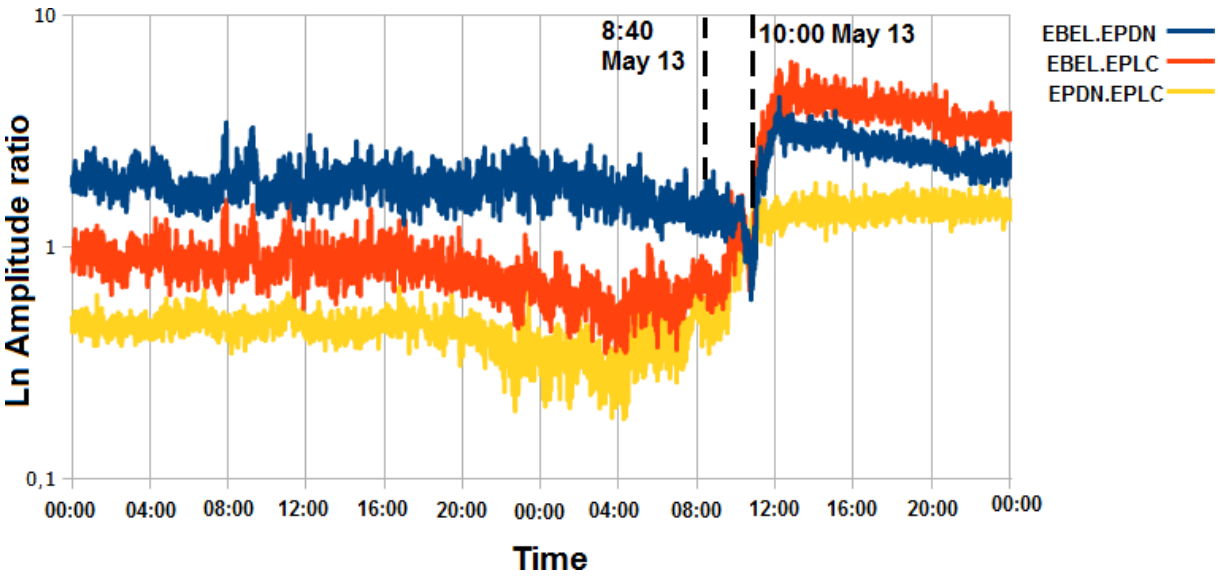

Figure 11. Seismic amplitude ratios on the logarithmic scale on 12 and 13 May 2008. Important periods are marked with black dashed lines.

5. Mann-Kendal trend test

We used the Mann-Kendall trend test to evaluate the uncertainty of the SARA method. This test is a nonparametric method that examines the existence of trends in time series. It was introduced by Mann [1945] and Kendall [1975] improved this method.

In this test, the Kendall correlation coefficient (τ) and statistical parameter p-value are calculated. The p-value is a probability that measures the records versus the null hypothesis. The p-value (<0.0001) shows that the null hypothesis is rejected and there is a possibility of a significant trend in the time series.

Kendall tau coefficient is the number of concordant pairs of observations (C) minus the number of discordant pairs of observations (U) with respect to a monotonic increasing time series is defined as follows:

$$\tau = \frac{C - U}{\frac{1}{2\big(n(n-1)\big)}} \tag{3}$$

where n is the number of data points and τ changes are in the range $-1 \leq \tau \leq 1$. If the amplitude ratios are almost constant, it gives a value close to zero, and if the amplitude ratios show an increasing or decreasing trend, the values are closer to ± 1.

This test was performed, with a 95 percent confidence level and the significance level $\alpha = 0.05$, on the amplitude ratios of 10 pairs of stations for the day of the eruption and the day before (12 and 13 May 2008). The results are reported in Table 2.

Pairs of stations	p-value	Kendall's tau	Sen's slope
EBEL.ECPN	<0.0001	0.498	0.488
EBEL.EPDN	<0.0001	0.182	0.261
EBEL.EPLC	<0.0001	0.208	0.858
ECCS.ECPN	<0.0001	0.154	0.001
ECCS.EPDN	<0.0001	0.147	0.010
ECCS.EPLC	<0.0001	0.146	0.01
EPDN.ECPN	<0.0001	0.560	0.295
ECPN.EPLC	0.898	0.002	0.002
EPDN.EPLC	<0.0001	0.349	0.549
EBEL.ECCS	<0.0001	0.266	83.178

Table 2. Mann-Kendall test coefficients for 10 pairs of stations.

This test is based on comparing hypothesis zero(H_0) and one (H_a) and finally accepting or rejecting hypothesis zero. Here H_0 means there is no trend in amplitude ratios and H_a means there is a trend in ratios. As the computed

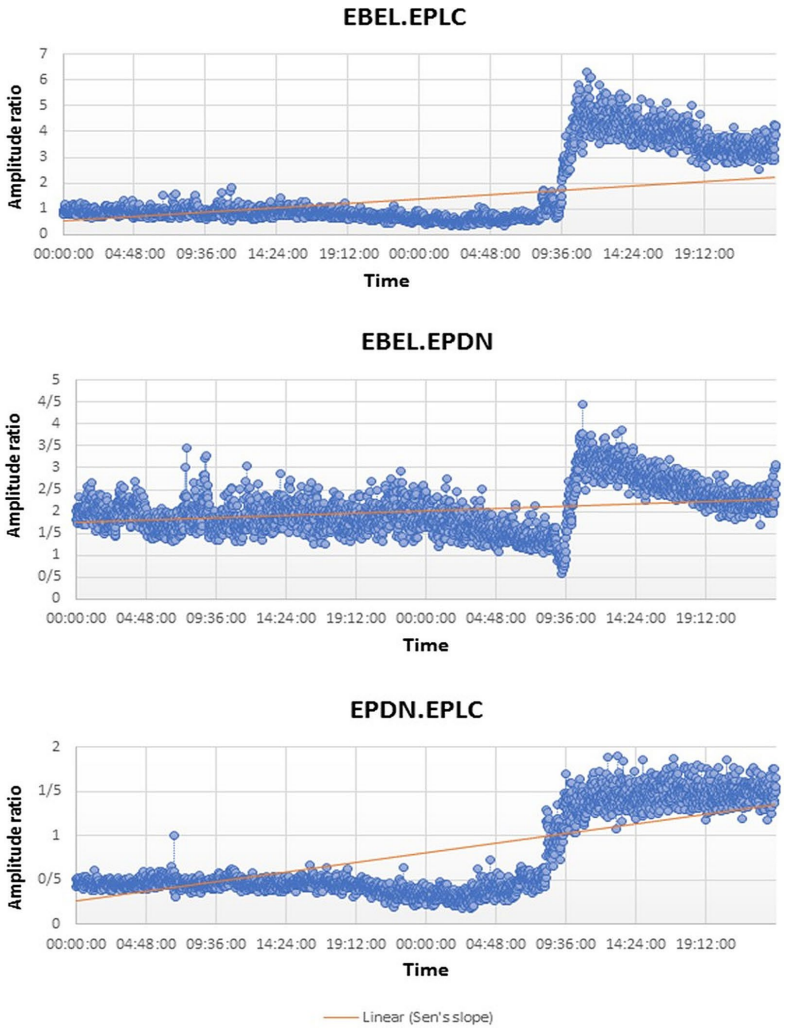

Figure 12. Time series of amplitude ratio for 3 pairs of stations on 12 and 13 May 2008.

p-value is lower than the significance level ($\alpha = 0.05$) for all pairs of stations except ECPN.EPLC (Table 2), one should reject the null hypothesis H_0, and accept the alternative hypothesis H_a. Also, due to the positive Kendall Tau coefficient, an increasing trend for all pairs of stations is approved. Therefore, in 90% of the pairs of investigated stations, we have witnessed a significant increase in the ratio of seismic amplitude recorded at pairs of stations starting from the day before the eruption.

The Sen's slope of the trends on the time series of the three pairs of stations studied in this paper is shown as a sample in Figure 12.

As shown in Figure 12, Sen's slope for all three pairs of stations is positive, which quantitatively confirms the increasing trend of amplitude ratios.

6. Discussion

Temporal changes in the ratio of seismic amplitudes can happen for two reasons: 1 – the law of attenuation and 2 – the change in the distance between the source and the receiver. Since this method uses a pair of independent and close stations, attenuation at this distance is unlikely to occur and the reason for the changes observed is related to the location of the seismic source, due to stress migration and magma migration. Each pair of stations in Figure 9 shows clear fluctuations in two separate periods. Around two hours before the main eruption, significant changes were observed in the amplitude ratio of the seismic waves as well as the location of the source (Figure 9). Although the whole seismic signal was recorded at the seismic stations used to analyze the amplitude ratio, the

results and changes observed were very consistent with the results of using the amplitude ratio of volcanic tremors for the same eruption (Figure 10) [Bonaccorso et al., 2011]. The first significant variation is detected on 10 May, at the same time as the lava fountaining at SEC crater, and the second stage of fluctuation starts between 12 and 13 May. To examine these changes more closely, the amplitude ratio was plotted on a logarithmic scale, for 12 and 13 May (Figure 11). Figure 11 shows a clear change in the amplitude ratios for all seismic station pairs and consequently, it shows significant seismic energy released approximately one day before the eruption; the most energetic stage occurred at 10:00 (GMT) on 13 May, coinciding with a strong seismic swarm that began at 8:40 (GMT).

With the onset of a seismic swarm, the ratio increased at EPDN/EPLC, but the ratios of the other two pairs of stations (EBEL/EPLC, EBEL/EPDN) first show a relatively sharp decrease and then increased again corresponding to lava flows (Figure 13). For both ratios including the EBEL, observations show that the seismicity is moving towards this station which is consistent with the location of the eruption (see Figure 1 for EBEL station position). As we know the location of the eruption, we can determine the possible path of the magma. The continuous increase in the ratio of EPDN/EPLC on the day of the eruption in Figure 13, which coincides with the onset of the seismic swarm, indicates the possibility of vertical migration of magma between these stations. On the other hand, the ratios decrease at other stations, in the same period, which could be a sign of lateral migration of magma to station EBEL (which is close to the eruption site).

We examine only the temporal evolution and the process of change instead of the actual values. However, the possible path of magma determined by this method is compliant with prior studies in this field [Aloisi et al., 2009; Bonaccorso et al., 2009; Wunderman., 2008].

Finally, SARA results have been combined with ground deformation results to furnish new insights; we have considered the double intrusive model of Aloisi et al. [2009] obtained by using tilt and GPS [Palano et al., 2010; Ferro et al., 2011; Gambino et al., 2014] data. They evidenced two dike intrusion sources: the first is an NNW oriented tensile dislocation (source 1 in Figure 13b), 1.6 km wide with an opening of about 1.0 meter close to the eruptive fractures; the second, with a width of 1 kilometer and an opening of 1.2 meters, located NW for the first model (source 2 in Figure 13b). This last dike intrusion did not reach the surface but caused a large fracture field within the north part of the summit region, consistent with the northward seismicity migration shown in Figure 3.

Figure 13 reports the EBEL/EPLC and EBEL/EPDN ratios during the morning of 13 May. These ratios show a particular pattern with phases of increasing and decreasing. EBEL/EPLC and EBEL/EPDN ratios (Figure 13) may suggest that the increasing phases may be related to source 1 as EBEL seismic energy is higher than EPLC and EPDN. Instead, during the decreasing phases, EPLC and EPDN seismic energy increased, suggesting that source 2 may have been predominant.

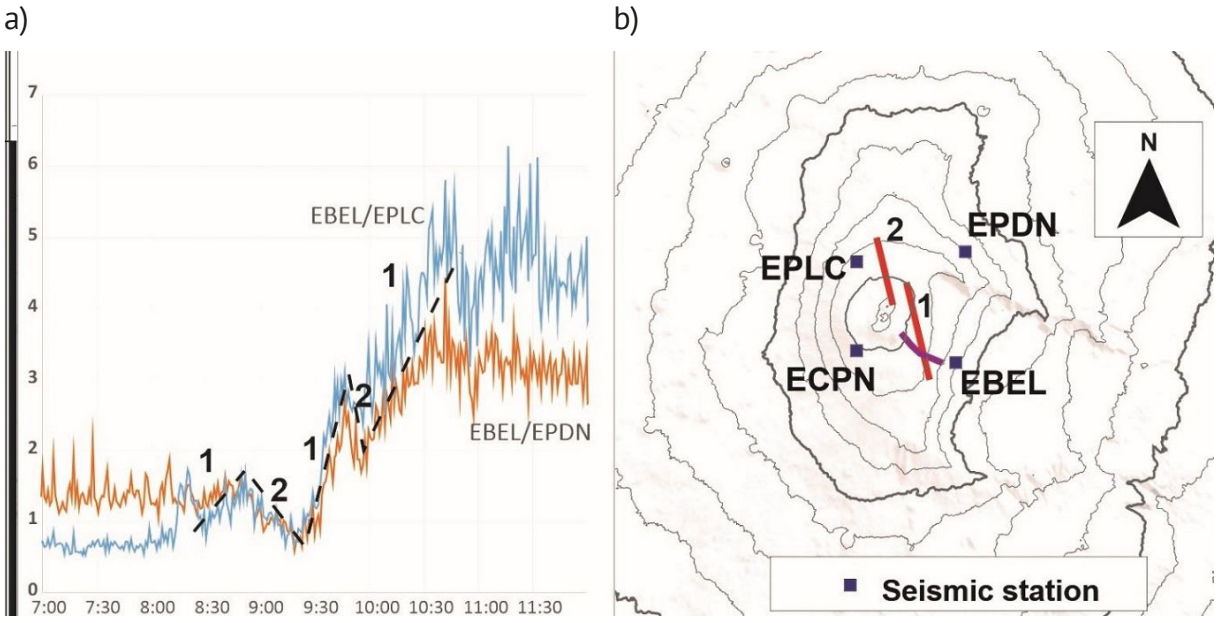

Figure 13. a) EBEL to EPLC and EBEL to EPDN ratios recorded during 7:00-12:00 GMT of 13 May. b) Dike sources modeled by Aloisi et al. [2009] (red lines) and the 2008 eruptive fissure (purple line).

7. Conclusions

Although the SARA method does not calculate the absolute values of seismic amplitudes, it provides a good insight into magma migration by examining the trend of changes in the amplitude ratio. We applied the SARA method using 8-days of data from three seismic stations near Mount Etna, and despite the limited data, the results were convincing and informative. Based on the analysis of the seismic amplitude ratios for the three mentioned stations used in this research, two significant changes came to light, the first of which relates to 10 May, a few hours before the lava fountain occurrence, and the second fluctuation, observed on 13 May, which could be interpreted as an indicator for the posterior magma migration. Quantitative analysis of the results using the Mann-Kendall test and Sens slope values also confirmed a significant increase in the ratio of seismic amplitude.

This easy and practical method could be widely and continuously adopted in observatories and used as a fast and permanent tool for monitoring volcanoes. We found that the SARA method has a number of advantages and a few limitations, the advantages being:

- Automatic determination of start and end time of seismic swarms and also seismic migration before the eruption.
- Tracking the trend of subsurface magma migration before eruptions, especially in shallower parts of volcanic structures.
- As shown in this research, the SARA method detects migration even in the absence of continuous earthquakes, so it is also useful for eruptions that are not associated with seismic events.
- As in this study, the magma migration was tracked using only 3 seismic stations close to the eruption location, implying that the SARA method is applicable even when a small number of seismic stations is available. Therefore, it could be useful for volcanos that lack advanced seismic stations networks.
- In this article, we did not limit ourselves to the use of volcanic tremors and used the whole recorded seismic signal in pairs of stations, and the results were similar to the use of tremors [Bonaccorso et al., 2011]. This method can be applied for volcanic sites where there is no complete continuous information about tremors.
- In this article, MsNoise open-source software was used to implement the SARA method at Mt. Etna volcano. This software can be connected directly to the database, automatically processing the data archive and performing the necessary calculations and categorization daily. By linking this software to the database of each volcanic station, this method can be implemented automatically and used to continuously make evaluations which could prove very useful for early warnings of the main eruption.

Despite the extraordinary advantages, mentioned above, the SARA method still has a few limitations:

- The efficacy of the method depends on the quality of the pre-information about the study area such as Quality Factors, and seismic velocities.
- Uncertainty of the method, like any other seismic locating method, depends on the signal-to-noise ratio, network configuration, and position of seismic sources. However, if stations are selected close to each other and close to the eruption site, these limitations can be attenuated.

Despite the limitations of the SARA method, this simple algorithm can be applied to a wide range of volcanoes throughout the world. Our future objective is to make this method smarter, using machine learning, and get a quick answer on the presence or absence of eruption-related migration and quick real-time assessment that could prove a powerful and intelligent tool for monitoring volcanoes.

8. References

Allard, P., B. Behncke, S. D. Amico, M. Neri and S. Gambino (2006). Mount Etna 1993-2005: anatomy of an evolving eruptive cycle, Earth. Sci. Rev., 78, 85-114, Doi: 10.1016/j.earscirev.2006.04.002.

Aloisi, M., A. Bonaccorso, F. Cannavò, S. Gambino, M. Mattia, G. Puglisi and E. Boschi (2009). A new dyke intrusion style for the Mount Etna May 2008 eruption modeled through continuous tilt and GPS data, Terra Nova, 21, 4, 316-321, Doi: 10.1111/j.1365-3121.2009. 00889. x.

Aloisi, M., S. Jin, F. Pulvirenti and A. Scaltrito (2017). The December 2015 Mount Etna eruption: An analysis of inflation/deflation phases and faulting processes, J. Geodyn., 107, 34-45, Doi: 10.1016/j.jog.2017.03.003.

Alparone, S., G. Barberi, O. Cocina, E. Giampaolo, C. Musumeci and D. Patanè (2012). Intrusive mechanism of the 2008-2009 Mt. Etna eruption: Constraints by tomographic images and stress tensor analysis, J. Volcanol. Geoth. Res., 229-230, 50-63, Doi: 10.1016/j.jvolgeores.2012.04.001.

Alparone, S., A. Maiolino, A. Mostaccio, A. Scaltrito, G. Ursino, S. Barberi, G. Amico, E. Di Grazia, C. Giampiccolo, L. Musumeci, L. Scarfì and L. Zuccarello (2015). Instrumental seismic catalogue of Mt Etna earthquakes (Sicily, Italy): ten years (2000–2010) of instrumental recordings, Ann. Geophys., 58, 4, Doi: 10.4401/ag-6591.

Barreca, G., A. Bonforte and M. Neri (2013). A pilot GIS database of active faults of Mt. Etna (Sicily): A tool for integrated hazard evaluation, J. Volcanol. Geotherm. Res., 251, 170-186, Doi: 10.1016/j.jvolgeores.2012.08.013.

Battaglia, J., V. Ferrazzini, T. Staudacher, K. Aki and J. Cheminée (2005a). Pre-eruptive migration of earthquakes at the Piton de la Fournaise volcano (Réunion Island), Geophys. J. Int., 161, 2, 549-558, Doi: 10.1111/j.1365-246X.2005.02606. x.

Battaglia, J., K. Aki and V. Ferrazzini (2005b). Location of tremor sources and estimation of lava output using tremor source amplitude on the Piton de la Fournaise volcano: 1. Location of tremor sources, J. Volcanol. Geotherm. Res., 147, 3, 268-290, Doi: 10.1016/j.jvolgeores.2005.04.005.

Battaglia, J. and K. Aki (2003). Location of seismic events and eruptive fissures on the Piton de la Fournaise volcano using seismic amplitudes, J. Geophys. Res. Solid Earth, 108, B8, 615-631, Doi: 10.1029/2002JB002193.

Behncke, B., S. Falsaperla, and S. Pecora (2009). Complex magma dynamics at Mount Etna revealed by seismic, thermal, and volcanological data, J. Geophys. Res. Solid Earth, 114, B03211, doi:10.1029/2008JB005882.

Bonaccorso, A., and M. Aloisi (2021). Tracking Magma Storage: New Perspectives From 40 Years (1980 - 2020) of Ground Deformation Source Modeling on Etna Volcano, Front. Earth Sci., 9, 171, Doi: 10.3389/feart.2021.638742.

Bonaccorso, A., A. Bonforte, S. Calvari, C. Del Negro, G. Di Grazia, G. Ganci, M. Neri, A. Vicari and E. Boschi (2011a). The initial phases of the 2008-2009 Mount Etna eruption: A multidisciplinary approach for hazard assessment, J. Geophys. Res. Solid Earth, 116, B3, Doi: 10.1029/2010JB007906.

Bonaccorso, A., A. Cannata, R.A. Corsaro, G. Di Grazia, S. Gambino, F. Greco, L. Miraglia, and A. Pistorio (2011b). Multi-disciplinary investigation on a lava fountain preceding a flank eruption: The 10 May 2008 Etna case, Geochem, Geophys. Geosyst., 12, 7, Doi: 10.1029/2010GC003480.

Cannata, A., G. Di Grazia, M. Aliotta, C. Cassisi, P. Montalto and D. Patanè (2013). Monitoring Seismo-volcanic and Infrasonic Signals at Volcanoes: Mt. Etna Case Study, Pure Appl. Geophys., 170, Doi: 170. 10.1007/s00024-012-0634-x.

Caudron, C., B. Taisne, Y. Kugaenko and V. Saltykov (2015). Magma migration at the onset of the 2012-13 Tolbachik eruption revealed by Seismic Amplitude Ratio Analysis, J. Volcanol. Geoth. Res., 307, 60-67, Doi: 10.1016/j.jvolgeores.2015.09.010.

Caudron, C., S. White, R. G. Green, J. Woods, T. Ágústsdóttir, C. Donaldson and B. Brandsdóttir (2018). Seismic amplitude ratio analysis of the 2014-2015 Bárðarbunga-Holuhraun Dike Propagation and Eruption, J. Geophys. Res. Solid Earth, 123, 264-276, Doi: 10.1002/2017JB014660.

Crisci, G. M., M.V. Avolio, B. Behncke, D. D'Ambrosio, S. Di Gregorio, V. Lupiano and W. Spataro (2010). Predicting the impact of lava flows at Mount Etna, Italy, J. Geophys. Res. Solid Earth, 115, B4, Doi: 10.1029/2009JB006431.

Del Pezzo, E., F. Bianco and E. Giampiccolo (2015). A reappraisal of seismic Q evaluated at Mt. Etna volcano. Receipt for the application to risk analysis, J. Seismol., 19, 105-119, Doi: 10.1007/s10950-014-9453-0.

De Plaen, R. S., A. Cannata, F. Cannavo, C. Caudron, T. Lecocq and O. Francis (2019). Temporal changes of seismic velocity caused by volcanic activity at Mt. Etna revealed by the autocorrelation of ambient seismic noise, Front. Earth Sci., 6, 251, Doi: 10.3389/feart.2018.00251.

Ferro, A., S. Gambino, S. Panepinto, G. Falzone, G. Laudani, and B. Ducarme (2011). High precision tilt observation at Mt. Etna Volcano (Italy), Acta Geophys., 59, 3, 618-632, Doi: 10.2478/s11600-011-0003-7.

Gambino, S., G. Falzone, A. Ferro and G. Laudani (2014). Volcanic processes detected by tiltmeters: A review of experience on Sicilian volcanoes, J. Volcanol. Geotherm. Res., 271, 43-54, Doi: 10.1016/j.jvolgeores.2013.11.007.

Gambino, S., G. Distefano, V., Maiolino, S. Gresta (2018). Seismic vs. geodetic moments at Mt. Etna volcano: A tool for a rapid understanding the eruptive behavior? J. Volcanol. Geotherm. Res., 367, 1-6, Doi:10.1016/j.jvolgeores.2018.10.012.

Giampiccolo, E., S. D'Amico, D. Patanè and S. Gresta (2007). Attenuation and Source Parameters of Shallow Microearthquakes at Mt. Etna Volcano, Italy, Bull. Seismol. Soc. Am., 97, 184-197, Doi: 10.1785/0120050252.

Hajian, A., F. Cannavò, F. Greco and G. Nunnari (2019). Classification of mount ETNA (ITALY) volcanic activity by Machine Learning Approaches, Ann. Geophys., 62,2, Doi: 10.4401/ag-8049.

Kendall, M., and J.D. Gibbons (1990). Rank Correlation Methods. Griffin, 5th edn. Oxford University Press, New York.

Laiolo M., M. Ripepe, C. Cigolini, D. Coppola, M. Della Schiava, R. Genco, L. Innocenti, G. Lacanna, E. Marchetti, F. Massimetti and M.C. Silengo (2019). Space- and Ground-Based Geophysical Data Tracking of Magma Migration in Shallow Feeding System of Mount Etna Volcano, Remote Sensing, 11, 10, 1182, Doi: 10.3390/rs11101182.

Larose, E., T. Planes, V. Rossetto and L. Margerin (2010). Locating a small change in a multiple scattering environment, Appl. Phys. Lett., 96, 20, Doi: 10.1063/1.3431269.

Lecocq, T., C. Caudron and F. Brenguier (2014). MSNoise, a Python package for computing and monitoring seismic velocity changes using ambient noise, Seismol. Res. Lett., 85, 715-726, Doi: 10.1785/0220130073.

Li, K.L., H. Sadeghisorkhani, G. Sgattoni, O. Gudmundsson and R. Roberts (2017). Locating tremor using stacked products of correlations, Geophys. Res. Lett., 44, 7, 3156-3164, Doi: 10.1002/2016GL072272.

Lo Giudice, E., G. Patanè, R. Rasà and R. Romano (1982). The structural framework of Mt. Etna, Società Geologica Italiana, 23, 125-158, Doi: 10.1016/S1464-1895(00)00108-3.

McNutt S.R. (1996) Seismic Monitoring and Eruption Forecasting of Volcanoes: A Review of the State-of-the-Art and Case Histories. In: Monitoring and Mitigation of Volcano Hazards. Springer, Berlin, 99-146, Doi:10.1007/978-3-642-80087-0-3.

Minakami, T. (1961). Study of eruptions and earthquakes originating from volcanoes (part 1 of 3) statistical relations between eruptions and earthquakes of Asama volcano, Int. Geol. Rev., 3, 8, 712-719, Doi: 10.1080/00206816109473633.

Morioka, H., H. Kumagai and T. Maeda (2017). Theoretical basis of the amplitude source location method for volcano-seismic signals, J. Geophys. Res. Solid Earth, 122, 6538-6551, Doi: 10.1002/2017JB013997.

Palano, M., M. Rossi, F. Cannavò, V. Bruno, M. Aloisi, D. Pellegrino, M. Pulvirenti, G. Siligato and M. Mattia (2010). Etn@ref: a geodetic reference frame for Mt. Etna GPS networks, Ann. Geophys., 53, 4, Doi: 10.4401/ag-4879.

Patanè, D., G. Di Grazia, A. Cannata, P. Montalto and E. Boschi (2008). Shallow magma pathway geometry at Mt. Etna volcano, Geochem. Geophys., 9, 12, Doi:10.1029/2008GC002131.

Rymer, H., F. Ferrucci and C.A. Locke (1998). Mount Etna: monitoring in the past, present, and future, Geol. Soc., 143, 335-347, Doi: 10.1144/GSL.SP.1998.143.01.

Shimozuru, D. (1971). Observation of volcanic eruption by an infrared radiation meter, Nature, 234, 5330, 457-459, Doi: 10.1038/234457a0.

Spina, L., A. Cannata, E. Privitera, S. Vergniolle, C. Ferlito, S. Gresta, P. Montalto and M. Sciotto (2014). Insights into Mt. Etna's Shallow Plumbing System from the Analysis of Infrasound Signals, Pure. Appl. Geophys., 172, 473-490, Doi: 10.1007/s00024-014-0884-x.

Subira, J., C. Caudron, A. Hubert, J. Barrière, A. Oth, and F. Kervyn (2019). Tracking magma movements in the Virunga volcanic province using seismic Amplitude Ratio Analysis (SARA), Geologica Belgica, 1374-8505.

Takemura, S., T. Furumura and T. Saito (2009). Distortion of the apparent S-wave radiation pattern in the high-frequency wavefield: Tottori-Ken Seibu, Japan, earthquake of 2000, Geophys. J. Int., 178, 2, 950-961, Doi: 10.1111/j.1365-246X.2009. 04210. x.

Takemura, S., M. Kobayashi and K. Yoshimoto (2016). Prediction of maximum P- and S-wave amplitude distributions incorporating frequency-and distance-dependent characteristics of the observed apparent radiation patterns, Earth Planets Space (EPS), 68, 1, 166, Doi: 10.1186/s40623-016-0544-8.

Ting Tan, C., B. Taisne, J. Neuberg and A. Basuki (2020). Real-time assessment of potential seismic migration within a monitoring network using Red-flag SARA, J. Volcanol. Geotherm. Res., 384, 31-47, Doi: 10.1016/j.jvolgeores.2019.07.004.

Taisne, B., F. Brenguierm F., Shapiro and V., Ferrazzini (2011). Imaging the dynamics of magma propagation using radiated seismic intensity, Geophys. Res. Lett., 38, Doi: 10.1029/2010GL046068.

Viccaro, M., F. Zuccarello, A. Cannata, M. Palano and S. Gresta (2016). How a complex basaltic volcanic system works: constraints from integrating seismic, geodetic, and petrological data at mount etna volcano during the July-August 2014 eruption, J. Geophys. Res., 121, 5659-5678, Doi: 10.1002/2016JB013164.

White, R. and W. McCausland (2016). Volcano-tectonic earthquakes: a new tool for estimating intrusive volumes and forecasting eruptions, J. Volcanol. Geotherm. Res., 309, 139-155, Doi: 10.1016/j.jvolgeores.2015.10.020.

Wunderman, R. (2008). Global Volcanism Program, Report on Etna (Italy), Bulletin of the Global Volcanism Network, 33, 5, Doi: 10.5479/si.GVP.BGVN200805-211060.

***CORRESPONDING AUTHOR: Alireza HAJIAN**,
Department of Physics, Najafabad Branch, Islamic Azad University, Najafabad, Iran,
e-mails: a.hajian@iaun.ac.ir, dralirezahajian@gmail.com